Atmospheric
Measurement
Techniques

Upper-troposphere and lower-stratosphere water vapor retrievals from the 1400 and 1900 nm water vapor bands

B. C. Kindel[1], P. Pilewskie[1,2], K. S. Schmidt[1], T. Thornberry[3,4], A. Rollins[3,4], and T. Bui[5]

[1]Laboratory for Atmospheric and Space Physics, University of Colorado, Campus Box 392, Boulder, CO, USA
[2]Department of Atmospheric and Oceanic Sciences, University of Colorado, Campus Box 311, Boulder, CO, USA
[3]NOAA Earth System Research Laboratory, Chemical Sciences Division, Boulder, CO, USA
[4]Cooperative Institute for Research in Environmental Sciences, University of Colorado, Boulder, CO, USA
[5]NASA Ames Research Center, Moffett Field, CA, USA

Correspondence to: B. C. Kindel (kindel@lasp.colorado.edu)

Abstract. Measuring water vapor in the upper troposphere and lower stratosphere is difficult due to the low mixing ratios found there, typically only a few parts per million. Here we examine near-infrared spectra acquired with the Solar Spectral Flux Radiometer (SSFR) during the first science phase of the NASA Airborne Tropical TRopopause EXperiment (ATTREX). From the 1400 and 1900 nm absorption bands we infer water vapor amounts in the tropical tropopause layer and adjacent regions between altitudes of 14 and 18 km. We compare these measurements to solar transmittance spectra produced with the MODerate resolution atmospheric TRANsmission (MODTRAN) radiative transfer model, using in situ water vapor, temperature, and pressure profiles acquired concurrently with the SSFR spectra. Measured and modeled transmittance values agree within 0.002, with some larger differences in the 1900 nm band (up to 0.004). Integrated water vapor amounts along the absorption path lengths of 3 to 6 km varied from 1.26×10^{-4} to 4.59×10^{-4} g cm^{-2}. A 0.002 difference in absorptance at 1367 nm results in a 3.35×10^{-5} g cm^{-2} change of integrated water vapor amounts; 0.004 absorptance change at 1870 nm results in 5.50×10^{-5} g cm^{-2} of water vapor. These are 27 % (1367 nm) and 44 % (1870 nm) differences at the lowest measured value of water vapor (1.26×10^{-4} g cm^{-2}) and 7 % (1367 nm) and 12 % (1870 nm) differences at the highest measured value of water vapor (4.59×10^{-4} g cm^{-2}). A potential method for extending this type of measurement from aircraft flight altitude to the top of the atmosphere is discussed.

1 Introduction

Water vapor in the stratosphere has important climatic (Forster and Shine, 2002; Solomon et al., 2010), dynamical (Joshi et al., 2006; Maycock et al., 2013), and chemical impacts (Stenke and Grewe, 2005). The long-term trends in water vapor have shown a general increase over the period of reliable measurements, starting in the 1970s with balloon-borne hygrometer measurements (Oltmans et al., 2000; Rosenlof et al., 2001; Hurst et al., 2011). Later satellite measurements from, for example, the Halogen Occultation Experiment (HALOE), extended these measurements to global scales from the geographically limited balloon measurements (e.g., Remsberg et al., 1996; Dessler and Kim, 1999). The record of stratospheric water vapor since 2000 has shown periods of both increasing and decreasing concentrations (Randel et al., 2004, 2006; Scherer et al., 2008; Fueglistaler, 2012; Nedoluha et al., 2013). The mechanisms driving changes in stratospheric water vapor concentrations are currently unresolved.

The transport of air from the troposphere to the stratosphere occurs mainly in the tropics (Brewer, 1949). Water vapor moving from the tropical troposphere to the stratosphere must pass through the so-called tropical tropopause layer (TTL) (Fueglistaler et al., 2009), characterized by very low temperatures. The TTL acts as a cold trap, "freeze drying" air as it passes through, limiting the entry of water vapor into the stratosphere (Brewer, 1949). Understanding the fate of water vapor as it encounters the TTL is one of the main sci-

ence objectives of the NASA Airborne Tropical TRopopause EXperiment (ATTREX).

The first ATTREX science flights were conducted on the NASA Global Hawk (GH) aircraft from NASA Dryden Flight Research Center at Edwards Air Force Base in southern California during February and March of 2013. The GH carried instruments that measured atmospheric state, composition, and radiation. Included in these were measurements of downwelling solar spectral irradiance, in situ water vapor mixing ratio, pressure, and temperature. In this work we examine the use of strong water vapor absorption bands in the near-infrared (NIR) spectrum to infer water vapor amounts across the TTL, in the upper troposphere and lower stratosphere (UT/LS). Observed NIR water vapor absorptances are compared to model predicted absorptances using in situ profiles of water vapor, pressure, and temperature as input to the atmospheric radiative transfer model MODTRAN5 (MODerate resolution atmospheric TRANsmission) version 5.3.2 (Berk et al., 2006).

In addition to the sensitivity to even very small amounts of water vapor, these bands have the additional benefit of being virtually free of molecular (Rayleigh) scattering and contain very little aerosol extinction. Aerosols can be a substantial source of error when using, for example, the 940 nm water vapor band as in the case of the POAM III (Lumpe et al., 2002; Lucke et al., 1999) or SAGE II (Chu et al., 1993; Rind et al., 1993; Chiou et al., 1997; Thomason, et al., 2004) satellite instruments. Aerosols also could be a source of error at these altitudes and wavelengths under elevated stratospheric levels (e.g., a Pinatubo-type event), but for background levels, like those encountered during ATTREX, they are of no concern. Clouds are a potential source of interference in these wavelength bands.

We also explore the potential use of these bands to infer the column stratospheric water vapor amounts from aircraft altitude to the top of the atmosphere (TOA) based on solar irradiance measurements from the GH and other high-flying aircraft.

2　Background – water vapor absorption in the solar spectrum

Water vapor is the strongest and most prevalent absorber of solar radiation in the Earth's atmosphere (Goody and Yung, 1989). The three fundamental water vapor bands occur at 2.66, 2.74, and 6.3 μm (∼ mid-infrared). Their combination and overtone bands in solar wavelengths extend from the very weakly absorbing bands in the visible to the relatively strong bands in the NIR centered near 1400 and 1900 nm; these are nearly always saturated at sea level.

In the troposphere, the concentration of water vapor decreases rapidly with height. At the tropopause, 16–18 km in the tropics, the mixing ratios are very small, typically a few ppmv, as compared to the surface where tropical water vapor
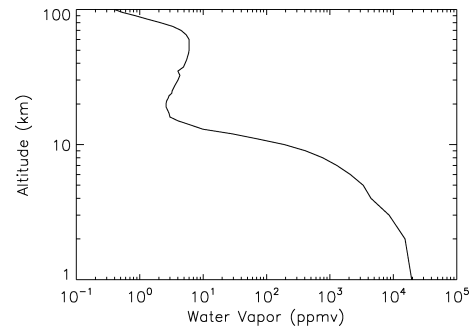

Figure 1. The vertical profile of water vapor mixing ratio used in the MODTRAN5 tropical atmosphere. At the tropopause (∼ 18 km), the mixing ratio is only a few ppmv.

mixing ratios are 20 000–25 000 ppmv. The vertical mixing ratio profile of water vapor used in the MODTRAN5 model for a tropical-type atmosphere is shown in Fig. 1.

Figure 2 shows the water vapor transmittance spectrum in the solar wavelength range for the entire tropical-type atmosphere (black spectrum), from sea level to the top of the atmosphere (defined here as 100 km altitude). The water vapor profile has a column-integrated amount of 4.11 g cm^{-2}. The spectrum was calculated at the Solar Spectral Flux Radiometer (SSFR) sampling and resolution. Also plotted on the left panel of Fig. 2 are modeled transmittances from 18 km (red spectrum), the greatest height that the tropical tropopause reaches, to TOA and from 14 km (blue spectrum) to TOA. These are the approximate maximum and minimum heights that the GH reached during its vertical profiling. At this height the only remaining appreciable water vapor absorption in the solar spectrum occurs at the two strongest bands centered near 1400 and 1900 nm and amounts to less than 0.03 in absorptance (1 minus transmittance). This is shown in an expanded view on the right-hand-side plot of transmittance of Fig. 2. Nevertheless, an instrument with sufficient signal-to-noise ratio (SNR) can make accurate measurements of water vapor even for absorptances over this small range, as will be demonstrated. The 1400 and 1900 nm water vapor bands are the focus of this paper.

3　Instrumentation

Measurements from three instruments were used for the present analysis work: the Solar Spectral Flux Radiometer, the NOAA water instrument (NW), and the Meteorological Measurement System (MMS). Each of these instruments is briefly described.

The SSFR (Pilewskie et al., 2003) is comprised of a pair of Zeiss monolithic spectrometers connected by fiber optics to a miniature integrating sphere that produces the cosine-weighted response required for measurements of irradiance. One integrating sphere measures the downwelling irradiance from the top of the aircraft, while the other measures the
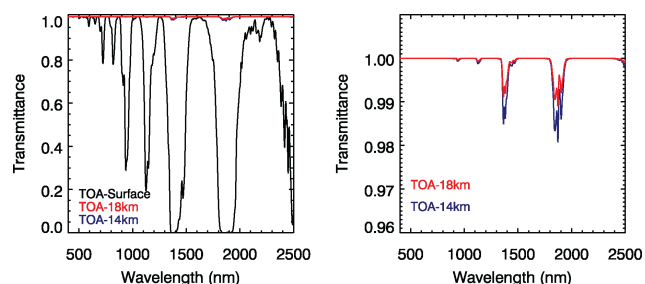
Figure 2. (left) Water vapor transmittance (modeled at SSFR sampling and resolution) in a tropical atmosphere is shown from the surface (black), 14 km (blue) and 18 km (red) to the top of the atmosphere. (right) An expanded plot of the water vapor absorption high in the atmosphere at 1400 and 1900 nm.

Figure 3. On the left is a map of the 2013 ATTREX flight lines. The black dots show the position of the vertical profiles used in this study. The numbers correspond to the first or second profile in that flight. Plotted on the right panel are examples of the profiles from the SF1. The SSFR transmittances are created using ratios of data averaged from right before and after the profile (red) and during level flight at the lowest altitude (blue).

upwelling irradiance from the bottom of the aircraft. The visible near-infrared, 256 pixel silicon detector array covers the wavelength range 350–1000 nm with 3 nm sampling and 8 nm full width at half maximum (FWHM) resolution. The 1000–2200 nm range is measured by a 256 pixel element In-GaAs array. This portion of the spectrum has 4.5 nm sampling and 12 nm FWHM resolution. The instrument records a complete spectrum every second (1 Hz). The absolute radiometric uncertainty is approximately 5 %; it is wavelength dependent with greater uncertainty with increasing wavelength. The absolute radiometric accuracy is limited by the NIST traceable standards of irradiance used to calibrate the instrument. The precision of the spectrometers is much better, about 0.1 % with averaging, as shown by the repeatability of the measurement and discussed in detail in Sect. 6. The work described in this paper relies solely on the precision of the spectrometers to derive atmospheric transmittance in the NIR.

The NOAA water vapor instrument is a two channel, closed-path, tunable diode laser absorption spectrometer. Different inlet geometries for the two channels allow for sampling of only water vapor into one channel and sampling of total water (the sum of water vapor, liquid, and water ice) into the second channel. In each channel a 2.7 µm tunable diode laser and an InAs detector are used to measure absorption over a mirror folded absorption path of 79 cm. The laser scans over strong (2693.82 nm) and weak (2694.06 nm) water vapor absorption lines. The strong line provides high sensitivity for measurement of low water vapor mixing ratios, while the weak line provides dynamic range for measurement at higher mixing ratios. The detection cells are operated at constant temperature and pressure to reduce the measurement uncertainty associated with line parameter changes. The overall measurement uncertainty is 5 % + 0.23 ppmv with a detection limit of 0.5 ppmv. The precision at 1 Hz is typically near 0.17 ppmv.

The MMS instrument measures aircraft position, altitude, attitude, winds, and, importantly for this work, pressure and temperature. Pressure is measured with a Paroscien-
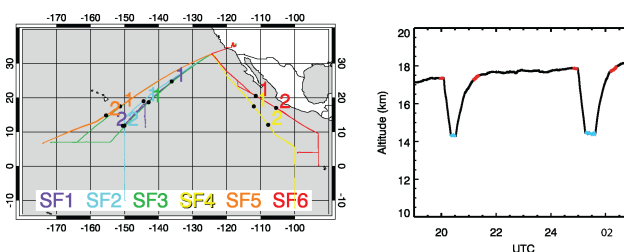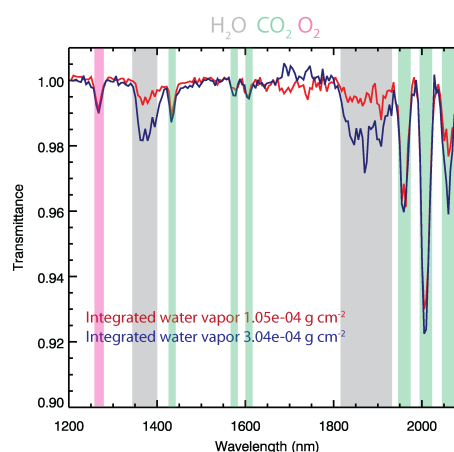

Figure 4. Transmittance spectra from the profiles shown in Fig. 2. Absorption band positions and widths are color coded: water vapor in gray, O_2 in magenta, and CO_2 in green. Integrated water vapor amounts in the figure indicate the corresponding water vapor column determined from the in situ measurements.

tific 6015A laboratory-grade sensor. The static temperature is measured with a Rosemount 102E4AL immersed open platinum wire. After a thorough systematic calibration process, including aerodynamic compensation from induced aircraft maneuvers, final static pressure accuracy is 0.3 hPa and static temperature accuracy is 0.3 K. The 1 Hz sampled MMS data were used in this study. Both sensors are NIST traceable and are periodically recalibrated by a certified laboratory.

4 Measurement technique

During the ATTREX 2013 field campaign, the GH flew southwest from NASA Dryden–Edwards Air Force Base in southern California. After transit to the tropical Pacific, the aircraft began a series of vertical profiles through the UT/LS between 14 and 18 km. From these profiles, those performed during daylight (11 total during the experiment period) were
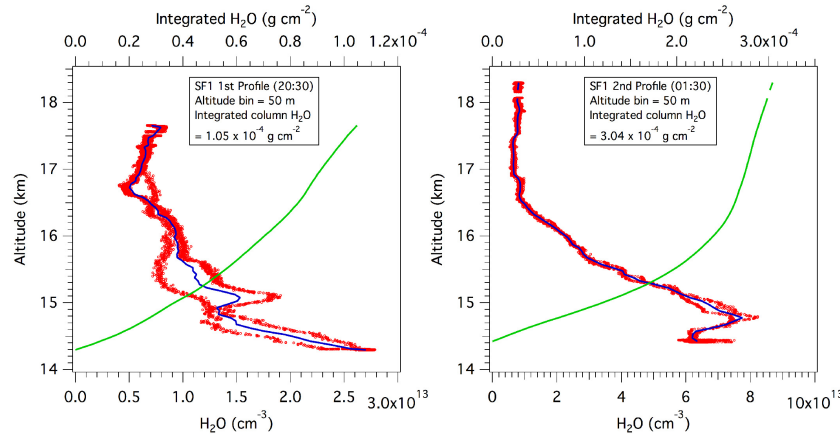
Figure 5. Water vapor number density profiles from the NOAA water instrument. The red points correspond to the in situ water vapor number densities during the descent and ascent for the two profiles. The blue line is the mean of the ascent and descent number densities. The green line is the integrated water vapor amounts (scale at the top of the plot). Note the large difference in the horizontal axis ranges and the integrated water vapor amounts between the two profiles.

selected for analysis. Figure 3 shows the map of flight lines of all six flights and the location of the vertical profiles on the left and the two profiles from the first science flight on 5 February 2013.

The derivation of atmospheric transmittance from the vertical profiles of solar spectral irradiance was straightforward: 5 to 10 min (300–600 spectra) of zenith SSFR data immediately prior to and after the descent from 18 km were averaged to give a robust measurement of the downward spectral irradiance at this altitude. The averaging both increases the SNR of the measurement and reduces the effects of attitude (pitch and roll) changes that are unavoidable during flight. The same averaging was performed during the period of level flight at the bottom of the profile near 14 km. These time periods are plotted in red (~ 18 km) and blue (~ 14 km) in Fig. 3. Transmittance spectra (T) were created from these averaged spectra by dividing the low-altitude average zenith downwelling irradiance ($F_{14\text{km}}$) by the high-altitude average zenith downwelling irradiance at ($F_{18\text{km}}$):

$$T = \frac{F_{14\text{km}}}{F_{18\text{km}}}. \tag{1}$$

The total absorption path length, denoted with the letter H in Fig. 6, depends on the altitude change of the aircraft profile (ΔZ) and the solar zenith angle (SZA) during the profile; H increases with increasing SZA. The vertical profiles during ATTREX were 3–4 km in Z; the range of solar zenith angles during the profiles produced values for H up to 5.93 km.

Figure 4 shows the resultant measured transmittance spectra from the first two profiles. The water vapor bands are shaded in gray, the CO_2 bands in green, and the oxygen band in red. Figure 5 shows the NW measurement of the water vapor number density and integrated H_2O amounts over the vertical profile. The measured integrated water vapor for the second profile was approximately three times greater

(Fig. 5, right-hand panel) than the first profile (Fig. 5, left-hand panel). In Fig. 4 the differences in the integrated water vapor paths are clearly indicated in the transmittances derived from the SSFR irradiances. The second profile, with the higher water vapor amount, had a significantly lower relative transmittance in the water vapor bands than the first profile.

5   Radiative transfer modeling

To assess the ability of SSFR measurements to infer water vapor across these relatively small absorption path lengths (3–6 km) and small water vapor amounts, radiative transfer modeling of the vertical profile transmittance was performed for comparison with the measured transmittances. The atmospheric radiative transfer model, MODTRAN5, was run using the profiles of water vapor concentration from the NW instrument and the profiles of static pressure and temperature from MMS as input. This is equivalent to radiosonde data required for MODTRAN modeling. MODTRAN5 was used to calculate the solar spectral irradiance at the altitudes of the top and bottom of each GH profile. The ratio of the two yields the transmittance spectrum in an identical manner to the SSFR measurements (Eq. 1).

MODTRAN5 uses a correlated-k model for gaseous absorption (Lacis and Oinas, 1991). This MODTRAN version of the band model includes updated line parameters from the HITRAN 2008 line database (Rothman et al., 2009). The water vapor continuum is modeled using the Clough–Kneizys Water Vapor Continuum version 2.4 (Clough et al., 1989).

The MODTRAN5 atmospheric profiles over the range of the GH profiles were modified to include the measurements of water vapor from NW and static pressure and temperature from MMS. Altitudes above and below the aircraft flight level were set to the tropical profile values. Over the range of
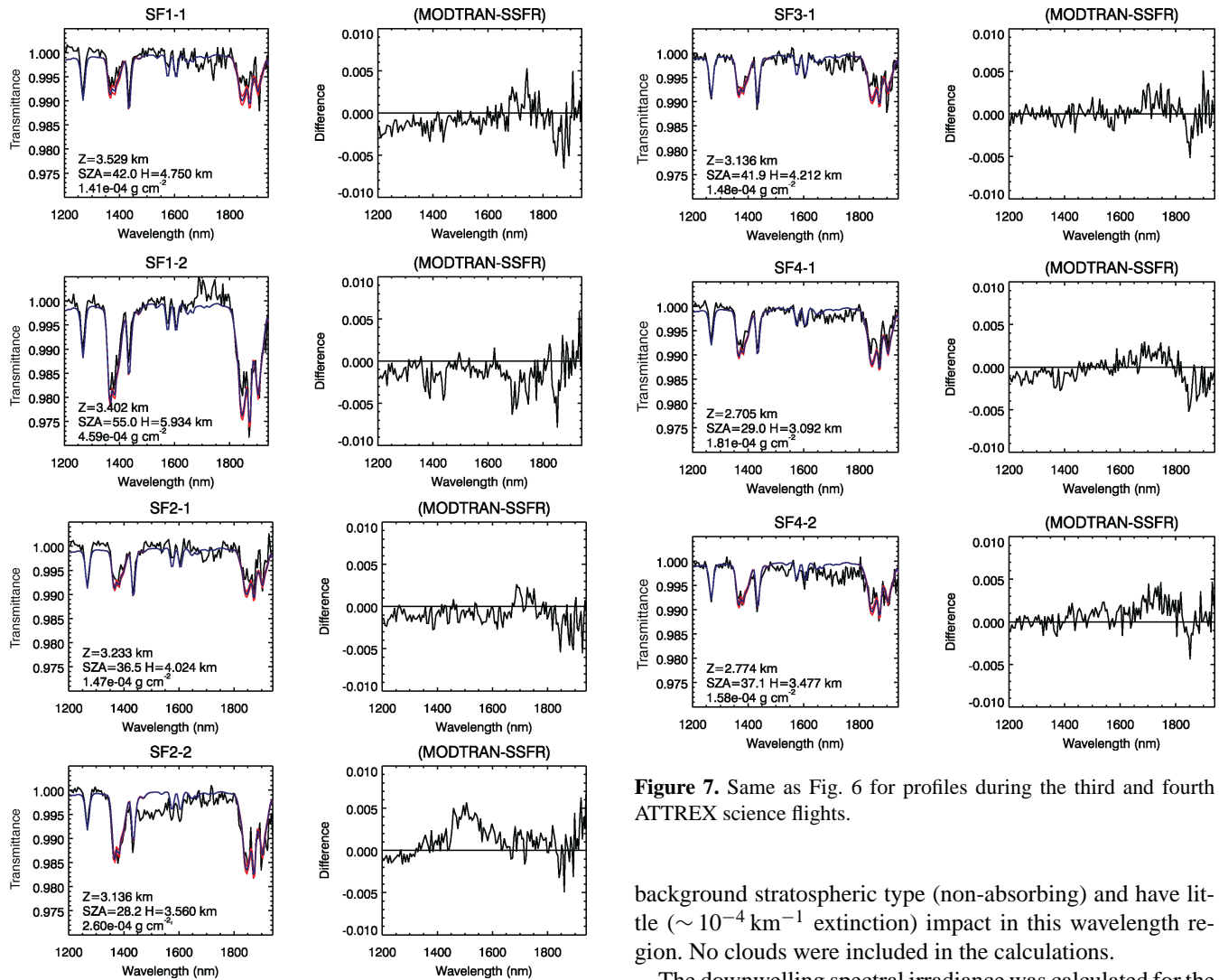
Figure 6. (left) Measured (black) and modeled (blue) transmittances for vertical profiles during the first and second ATTREX science flights are plotted. The red traces show plus and minus 1 standard deviation of the measured transmittance. (right) Difference between the measured and modeled transmittances. The vertical profile distance Z, the solar zenith angle SZA, the absorption path length H, and the integrated water vapor amounts are given in the left-hand plots.

Figure 7. Same as Fig. 6 for profiles during the third and fourth ATTREX science flights.

the aircraft profile, the model atmospheric levels were set to every 250 m, resulting in about 12 levels for each profile. The water vapor number densities were linearly interpolated to the model levels (e.g., 14.250, 14.500, 14.750 km) and were scaled to ensure that the integrated water vapor amount in the model (lower vertical resolution) matched that of the integrated NW measurements (higher vertical resolution). The solar zenith angles were calculated using the time and position of the GH for the high and low altitudes, and the important geometrical parameters for each transmittance spectrum are given in Figs. 6–8. Aerosols are the MODTRAN
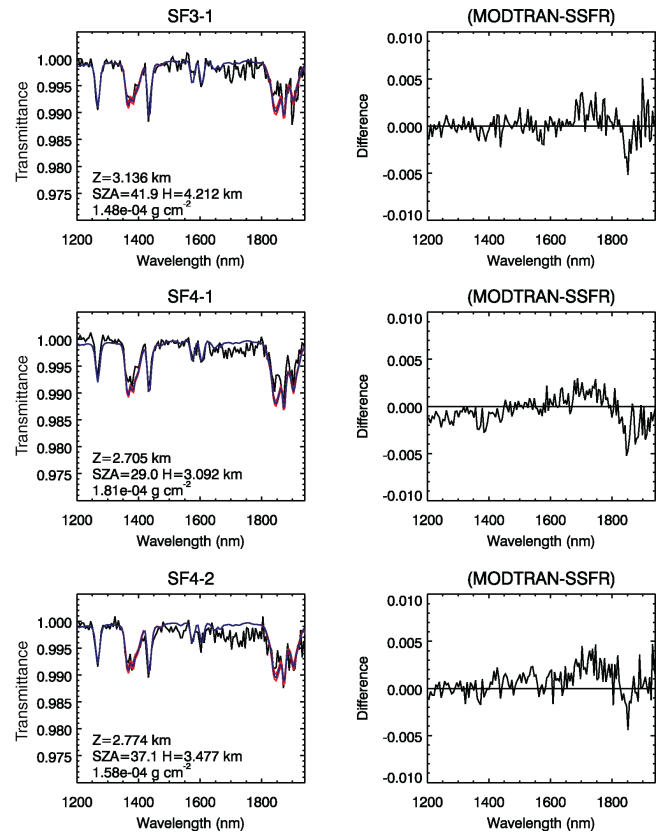
background stratospheric type (non-absorbing) and have little ($\sim 10^{-4}\,\mathrm{km}^{-1}$ extinction) impact in this wavelength region. No clouds were included in the calculations.

The downwelling spectral irradiance was calculated for the mean of the high-altitude and low-altitude legs of the GH profile, and the ratio of the two resulted in the atmospheric transmittance over the absorption path length

To estimate the effects of the water vapor spatial variability on the calculated transmittance spectra, water vapor measurement variation was propagated into the model by including ± 1 standard deviation of NW water vapor number densities in the model profiles. The model was run at $1\,\mathrm{cm}^{-1}$ sampling and $2\,\mathrm{cm}^{-1}$ resolution. MODTRAN spectra were spectrally convolved with the slit function of the SSFR for direct comparison with the measurements.

6 Results

In Figs. 6, 7, and 8 the measured and modeled transmittance spectra for all 11 profiles included in this study are plotted. The individual profiles are labeled SF (science flight) followed by the science flight number and the profile number. For example, SF2-2 corresponds to science flight number two (9 February 2013) and the second profile during that flight.
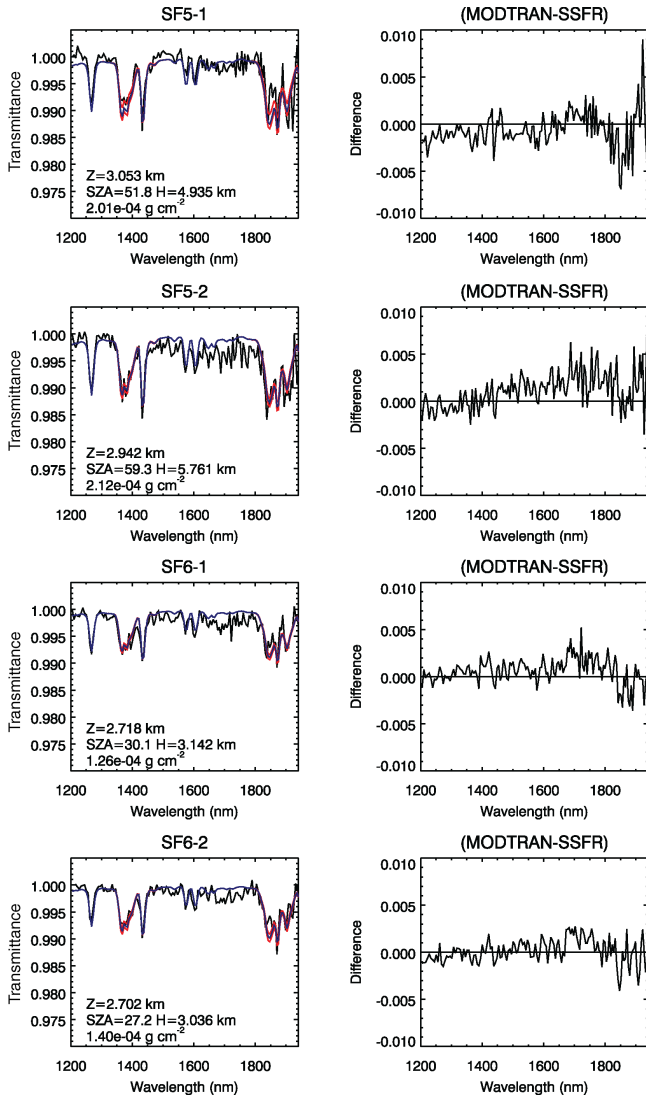
Figure 8. Same as Fig. 6 for profiles during the fifth and sixth AT-TREX science flights.

Figure 9. The mean (black) and standard deviation (red) difference (MODTRAN minus SSFR) spectra are plotted for the 11 profiles.

There were two daylight profiles per flight with the exception of the third flight, which had only one profile.

The mean SSFR spectra are plotted in black and the model spectra in blue. The modeled spectra at ±1 standard deviation of measured water vapor are shown in red. In general, the spatial variation in the water vapor profiles has little effect on the computed transmittance spectra, 0.001 or less, and indeed it is difficult to distinguish the mean spectra in blue from the standard deviation spectra in red in most of the plots.

The right-hand columns in Figs. 6, 7, and 8 show the measured–modeled residual spectra. In general, measured and modeled transmittances agree to within 0.002 in the 1400 nm water band and 0.003 to 0.004 in the 1900 nm band. Figure 9 shows the mean and standard deviation difference spectrum for the 11 cases. The MODTRAN5-computed absorptance is slightly greater than that measured by SSFR in
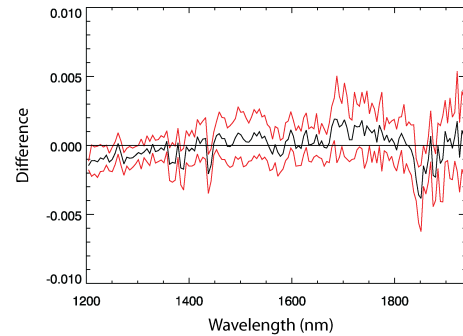
both the 1400 and 1900 nm bands. The largest consistent discrepancy occurs at 1849 nm, where the mean difference of all cases is nearly 0.004 (see Fig. 9). Most of the 1900 nm band agrees to within 0.002 or better, as does the entire 1400 nm band.

In SF2-2 the SSFR spectrum shows an unusually large discrepancy (up to 0.005) in the 1450 to 1600 nm wavelength range compared to MODTRAN. This is indicative of ice absorption and was the result of passing through a cloud during the profile. A significant advantage of a spectral measurement such as this is to identify just such events. Despite the presence of the cloud, which was optically thin, the agreement in the water vapor bands is remarkably good. Nevertheless, the water vapor retrievals are best restricted to clear sky conditions and clouds do have the potential to introduce significant error. We include it here to demonstrate how clouds can potentially be identified from SSFR measurements themselves.

Note that the measurements fall very close, to within 0.001 of unity, in the spectral regions free of molecular absorption, for example around 1300 nm (Fig. 9). The atmosphere at these heights and wavelengths is essentially transparent. This confirms the radiometric precision of the instrument is about 0.1 % with averaging of the spectra. At longer wavelengths, the differences become slightly greater (∼ 0.002) due to the lower SNR of the measurement. Solar irradiance rapidly decreases with wavelength in the NIR.

The results of the MODTRAN5 and SSFR water vapor transmittances and absorptances are summarized in Fig. 10. The top two plots show model calculations of a water vapor transmittance spectrum at SSFR resolution. The positions of the strongest absorption wavelength in each band, at 1367 nm (left) and 1870 nm (right), are indicated with a red line. In the second row, the values of absorptance from SSFR and MOD-TRAN5 at these wavelengths are plotted against each other for the 11 cases. In the bottom row, the absorptance is plotted against the line-of-sight-integrated water vapor amounts for both the MODTRAN and SSFR absorptances. The correlation between MODTRAN modeled and SSFR measured absorptances is quite good. The agreement for the higher water
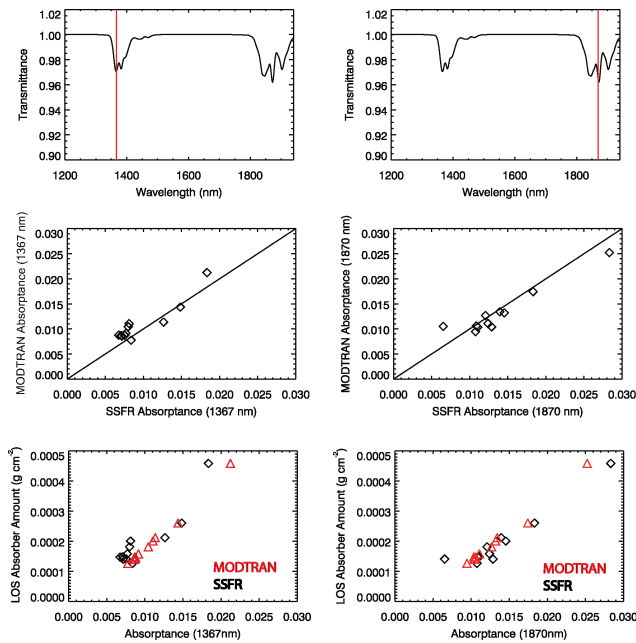
Figure 10. The top plots show modeled water vapor transmittance with the strongest part of each band indicated with a red vertical line. The middle panels show plots of SSFR measured versus MODTRAN-predicted absorptances at these wavelengths. The bottom panels show the measured and modeled absorptances plotted versus the line-of-sight-integrated water vapor amount.

vapor amounts is better, which is to be expected; the higher the water vapor amount the greater the absorptance and the signal.

7 Stratospheric water vapor

The results of this work thus far have focused on aircraft measurements during vertical profiles of a few kilometers in the UT/LS. The radiative transfer modeling using in situ measured profiles of water vapor amount has demonstrated that absorptance in the strong bands of water vapor at 1400 and 1900 nm can be used to infer water vapor amounts over short path lengths (3–6 km) and small water vapor mixing ratios (a few ppmv). Here we investigate the potential of using SSFR measurements to infer the column water vapor amount from downwelling irradiance from aircraft altitude to the top of the atmosphere.

The proposed technique relies on the transparency of the atmosphere at wavelengths surrounding the water vapor bands. A transmittance spectrum is created by fitting a model TOA solar spectrum to wavelengths near, but outside of the water vapor bands at 1400 and 1900 nm. An example is shown in Fig. 11.

MODTRAN5-modeled solar irradiances at 20, 18, 16, and 14 km are shown in the top left panel of Fig. 11 along with the TOA solar spectrum (Kurucz, 1995). The sun is directly over-

head, creating the shortest possible absorption path lengths at these altitudes. In the top right panel, the transmittance spectrum for the path from the TOA to each altitude is plotted. To produce these transmittance spectra, first the TOA solar spectrum was scaled to match downwelling irradiance spectrum at the wavelengths 1301, 1516, and 1756 nm, indicated by the three black vertical lines in the transmittance spectra, where the transmittance is very close to unity. The ratio of the scaled TOA solar spectrum to the downwelling irradiance produces a transmittance spectrum. The scaling of the TOA spectrum is a simple gain across all wavelengths; no wavelength-dependent (shape) changes were made. The mean deviation from a transmittance of unity for all altitudes at the three wavelengths is 0.001, which is approximately equivalent to the measurement uncertainty. Thus the impact on the retrieval of water vapor is negligible.

In the lower right panel of Fig. 11 the integrated water vapor amount is plotted against the absorptance for the 1367 and 1870 nm bands. Over this small range of water vapor amount, the absorptance is very nearly linear. A linear fit to the absorptance and integrated water vapor amount for this range of water vapor gives the following two equations for the two wavelengths:

$$H_2O_{g\,cm^{-2}} = 1.76 \times 10^{-2} \cdot \left(Absorptance_{1367nm}\right)$$
$$- 1.70 \times 10^{-6}, \tag{2}$$

$$H_2O_{g\,cm^{-2}} = 1.49 \times 10^{-2} \cdot \left(Absorptance_{1870nm}\right)$$
$$- 4.56 \times 10^{-6}. \tag{3}$$

The intercepts of these equations are very near zero ($\sim 10^{-6}$) as expected; zero absorptance should correspond to zero water vapor amount. These linear fits provide a simple method for estimating the uncertainty of the SSFR absorptance measurement in terms of water vapor amount. For instance, an uncertainty of 0.002 in the SSFR absorptance at 1367 nm (the mean difference between the model and the measurements) corresponds to a 3.35×10^{-5} g cm^{-2} integrated water vapor change. Similarly, a 0.004 change in absorptance at 1870 nm results in a 5.51×10^{-5} g cm^{-2} change in water vapor amount. These linear relationships are not valid for larger amounts of water vapor found at lower altitudes. As the water amount increases, individual lines within the bands become saturated and the absorptance is no longer linear with water vapor amount.

In practice, a model TOA spectrum would be fit at these wavelengths to a SSFR spectrum and the ratio calculated. A pre-calculated lookup table of absorptances generated from a range of water vapor amounts, solar zenith angles, and altitudes would be used to determine the integrated water vapor amount above the aircraft. This retrieval could be undertaken in near real-time from aircraft equipped with high-bandwidth downlinks. This type of real-time retrieval is becoming more common with the introduction of such satellite downlinks to the NASA ER-2 and Global Hawk aircraft. In the lower left
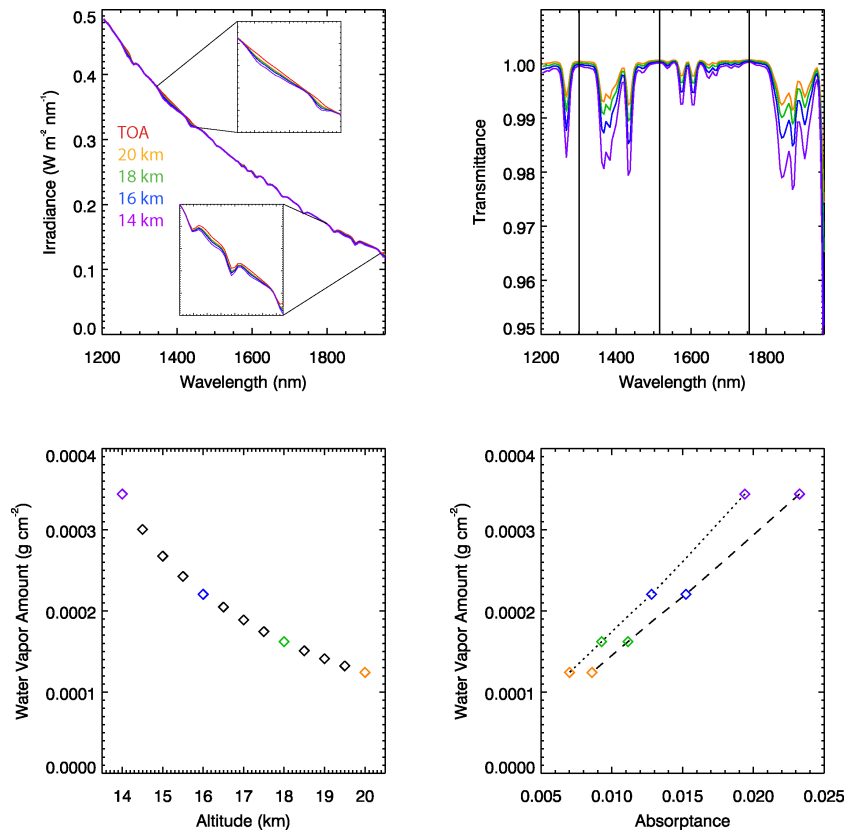
Figure 11. In the top left panel, modeled irradiances with expanded plots of the 1400 and 1900 water vapor bands are plotted. The top right panel shows the transmittance spectra for each altitude. In the bottom left panel, integrated water vapor amounts from the various altitudes to the TOA are plotted. In the bottom right panel, the integrated water vapor amount is plotted as a function of absorptance at 1367 (dotted line) and 1870 nm (dashed line).

panel of Fig. 11, the water vapor amounts corresponding to the transmittances are plotted as a function of altitude. The values for the transmittances plotted in the top left panel are color coded. The range of water vapor amounts fall within the same range as those measured in the UT/LS during AT-TREX, indicating that stratospheric water vapor amounts are within the capability of the SSFR to measure. However, this will require that radiometric calibration of the instrument be modified to remove the water vapor surrounding the laboratory setup. The water vapor bands can have significant (1–2 %) absorption even over the path length (50 cm) from the NIST irradiance standard to the light collector (Kindel et al., 2001). The absorption by water vapor in the laboratory radiometric calibration of the SSFR has likely masked the small absorption in previous SSFR measurements.

8   Summary and conclusions

Water vapor in the upper atmosphere has important climatic, dynamical and chemical impacts on the Earth's atmosphere. The accurate measurement of water vapor in the upper troposphere and stratosphere is important in quantifying these

impacts. Airborne measurements near or at the TTL have the ability to probe the mechanisms of water vapor transport into stratosphere at vertical and horizontal scales and with accuracies that are unobtainable by either balloon or satellite measurements. The GH flights made during ATTREX should provide insight into water vapor in the UT/LS and the mechanisms of its transport into the stratosphere.

In this work we have examined the use of the strong water vapor bands in the solar spectrum to infer water vapor amounts in the UT/LS. This work, unlike most previous work using solar transmittance-type retrievals, used aircraft in situ measurements of water vapor vertical profiles over very small mixing ratios, a few ppmv, to predict the transmittance and compare with measurements. Most solar transmittance-type retrievals have little if any independent validation of water vapor amount, vertical distribution, pressure, or temperature profile (Schwab et al., 1996; Harries et al., 1996; Taha et al., 2004).

Comparisons of modeled and measured transmittance spectra for 11 cases resulted in spectra that agreed to generally 0.002 in transmittance with deviations up to 0.004 in some channels of the 1900 nm band. The measurement

uncertainly is approximately 0.001 as demonstrated by the repeatability of the measurements in non-absorbing wavelengths (e.g., 1300 nm). This increases to 0.002 at longer wavelengths where the SNR is not as high.

A technique for inferring water vapor from downwelling airborne solar spectral irradiance has been outlined. This technique relies on the use of wavelengths surrounding the strong NIR water vapor bands where the atmosphere is essentially transparent. Radiative transfer modeling of water vapor transmittance from altitudes of 14 to 20 km indicate that integrated water vapor amounts, and thus the transmittances from these altitudes to the TOA, fall in a similar range to the shorter path lengths examined in this work. This technique could potentially produce near-real-time retrievals of aircraft-to-TOA water vapor amounts. The absorption of other gases in this wavelength range such as oxygen and carbon dioxide might provide important constraints on the radiative transfer modeling and information on potential contamination by aerosols or clouds. More extensive radiative transfer modeling is required to investigate their usefulness. Work is required to modify the radiometric calibration to remove the effects of water vapor in the laboratory and forward radiative transfer modeling to determine the integrated water vapor amounts from the measurement of transmittance.

References

Berk, A., Anderson, G. P., Acharya, P. K., Bernstein, L. S., Muratov, L., Lee, J., Fox, M., Adler-Golden, S. M., Chetwynd, J. H., Hoke, M. L., Lockwood, R. B., Gardner, J. A., Cooley, T. W., Borel, C. C., Lewis, P. E., and Shettle, E. P.: MODTRAN5: 2006 Update, Proc. SPIE, 6233, 62331F, doi:10.1117/12.665077, 2006.

Brewer, A. W.: Evidence for a world circulation provided by the measurements of helium and water vapour distribution in the stratosphere, Q. J. Roy. Meteorol. Soc., 75, 351–363, doi:10.1002/qj.49707532603, 1949.

Chiou, E. W., McCormick, M. P., and Chu, W. P.: Global water vapor distributions in the stratosphere and upper troposphere derived from 5.5 years of SAGE II observations (1986–1991), J. Geophys. Res., 102, 19105–19118, doi:10.1029/97JD01371, 1997.

Chu, W. P., Chiou, E. W., Larsen, J. C., Thomason, L. W., Rind, D., Buglia, J. J., Oltmans, S., McCormick, M. P., and McMaster, L. M.: Algorithms and sensitivity analyses for Stratospheric

Aerosol and Gas Experiment II water vapor retrieval, J. Geophys. Res., 98, 4857–4866, doi:10.1029/92JD01628, 1993.

Clough, S. A., Kneizys, F. X., and Davies, R. W.: Line shape and the water vapor continuum, Atmos. Res., 23, 229–241, 1989.

Dessler, A. E. and Kim, H.: Determination of the amount of water vapor entering the stratosphere based on Halogen Occultation Experiment (HALOE) data, J. Geophys. Res., 104, 30605–30607, doi:10.1029/1999JD900912, 1999.

Fueglistaler, S.: Stepwise changes in stratospheric water?, J. Geophys. Res., 117, D13302, doi:10.1029/2012JD017582, 2012.

Forster P. M. and Shine, K. P.: Assessing the climatic impacts of trends in stratospheric water vapour, Geophys. Res. Lett., 29, 1086–1089, 2002.

Fueglistaler, S., Dessler, A. E., Dunkerton, T. J., Folkins, I., Fu, Q., and Mote, P. W.: Tropical tropopause layer, Rev. Geophys., 47, RG1004, doi:10.1029/2008RG000267, 2009.

Goody, R. M. and Yung, Y. L.: Atmospheric radiation: theoretical basis, Oxford University Press, New York, 1989.

Harries, J. E., Russell III, J. M., Tuck, A. F., Gordley, L. L., Purcell, P., Stone, K., Bevilacqua, R. M., Gunson, M., Nedoluha, G., and Traub, W. A.: Validation of measurements of water vapor from the Halogen Occultation Experiment (HALOE), J. Geophys. Res., 101, 10205–10216, doi:10.1029/95JD02933, 1996.

Hurst, D. F., Oltmans, S. J., Vömel, H., Rosenlof, K. H., Davis, S. M., Ray, E. A., Hall, E. G., and Jordan, A. F.: Stratospheric water vapor trends over Boulder, Colorado: Analysis of the 30 year Boulder record, J. Geophys. Res., 116, D02306, doi:10.1029/2010JD015065, 2011.

Joshi, M. M., Charlton, A. J., and Scaife, A. A.: On the influence of stratospheric water vapor changes on the tropospheric circulation, Geophys. Res. Lett., 33, L09806, doi:10.1029/2006GL025983, 2006.

Kindel, B. C., Qu, Z., and Goetz, A. F. H.: Direct solar spectral irradiance and transmittance measurements from 350 to 2500 nm, Appl. Optics, 40, 3483–3494, doi:10.1364/AO.40.003483, 2001.

Kurucz, R. L.: The Solar Irradiance by Computation, Proc. of the 17th Ann. Rev. Conf. on Atmos. Trans. Models, edited by: Anderson, G. P., Picard, R. H., and Chetwynd, J. H., PL/-TR-95-2060, Special Reports, No. 274, Pl. 332, Phillips Laboratory, Geophysics Directorate, MA, May, 1995.

Lacis, A. A. and Oinas, V.: A description of the correlated k distribution method for modeling nongray gaseous absorption, thermal emission, and multiple scattering in vertically inhomogeneous atmospheres, J. Geophys. Res., 96, 9027–9063, doi:10.1029/90JD01945, 1991.

Lucke, R. L., Korwan, D. R., Bevilacqua, R. M., Hornstein, J. S., Shettle, E. P., Chen, D. T., Daehler, M., Lumpe, J. D., Fromm, M. D., Debrestian, D., Neff, B., Squire, M., König-Langlo, G., and Davies, J.: The Polar Ozone and Aerosol Measurement (POAM) III instrument and early validation results, J. Geophys. Res., 104, 18785–18799, doi:10.1029/1999JD900235, 1999.

Lumpe, J. D., Bevilacqua, R. M., Hoppel, K. W., and Randall, C. E.: POAM III retrieval algorithm and error analysis, J. Geophys. Res., 107, 4575, doi:10.1029/2002JD002137, 2002.

Maycock, A. C., Joshi, M. M., Shine, K. P., and Scaife, A. A.: The circulation response to idealized changes in stratospheric water vapor, J. Climate, 26, 545–561, doi:10.1175/JCLI-D-12-00155.1, 2013.

Nedoluha, G. E., Michael Gomez, R., Allen, D. R., Lambert, A., Boone, C., and Stiller, G.: Variations in middle atmospheric water vapor from 2004 to 2013, J. Geophys. Res. Atmos., 118, 11285–11293, doi:10.1002/jgrd.50834, 2013.

Oltmans, S. J., Vömel, H., Hofmann, D. J., Rosenlof, K. H., and Kley, D.: The increase in stratospheric water vapor from balloon-borne, frost point hygrometer measurements at DC and Boulder, Colorado, Geophys. Res. Lett., 27, 3453–3456, 2000.

Pilewskie, P., Pommier, J., Bergstrom, R. W., Gore, W., Howard, S., Rabette, M., Schmid, B., Hobbs, P. V., and Tsay, S. C.: Solar spectral radiative forcing during the Southern African Regional Science Initiative, J. Geophys. Res., 108, 8486, doi:10.1029/2002JD002411, 2003.

Randel, W. J., Wu, F., Oltmans, S. J., Rosenlof, K., and Nedoluha, G. E.: Interannual Changes of Stratospheric Water Vapor and Correlations with Tropical Tropopause Temperatures, J. Atmos. Sci., 61, 2133–2148, doi:10.1175/1520-0469(2004)061<2133:ICOSWV>2.0.CO;2, 2004.

Randel, W. J., Wu, F., Vömel, H., Nedoluha, G. E., and Forster, P.: Decreases in stratospheric water vapor after 2001: Links to changes in the tropical tropopause and the Brewer-Dobson circulation, J. Geophys. Res., 111, D12312, doi:10.1029/2005JD006744, 2006.

Remsberg, E. E., Bhatt, P. P., and Russell III, J. M.: Estimates of the water vapor budget of the stratosphere from UARS HALOE data, J. Geophys. Res., 101, 6749–6766, doi:10.1029/95JD03858, 1996.

Rind, D., Chiou, E.-W., Chu, W., Oltmans, S., Lerner, J., Larsen, J., McCormick, M. P., and McMaster, L.: Overview of the Stratospheric Aerosol and Gas Experiment II water vapor observations: Method, validation, and data characteristics, J. Geophys. Res., 98, 4835–4856, doi:10.1029/92JD01174, 1993.

Rosenlof, K. H., Oltmans, S. J., Kley, D., Russell, J. M., Chiou, E.-W., Chu, W. P., Johnson, D. G., Kelly, K. K., Michelsen, H. A., Nedoluha, G. E., Remsberg, E. E., Toon, G. C., and McCormick, M. P.: Stratospheric water vapor increases over the past half-century, Geophys. Res. Lett., 28, 1195–1198, doi:10.1029/2000GL012502, 2001.

Rothman, L. S., Gordon, I. E., Barbe, A., Benner, D. C., Bernath, P. F., Birk, M., Boudon, V., Brown, L. R., Campargue, A., Champion, J.-P., Chance, K., Coudert, L. H., Dana, V., Devi, V. M., Fally, S., Flaud, J.-M., Gamache, R. R., Goldman, A., Jacquemart, D., Kleiner, I., Lacome, N., Lafferty, W., Mandin, J.-Y., Massie, S. T., Mikhailenko, S. N., Miller, C. E., Moazzen-Ahmadi, N., Naumenko, O. V., Nikitin, A. V., Orphal, J., Perevalov, V. I., Perrin, A., Predoi-Cross, A., Rinsland, C. P., Rotger, M., Simeckova, M., Smith, M. A. H., Sung, K., Tashkun, S. A., Tennyson, J., Toth, R. A., Vandaele, A. C., and Vander Auwera, J.: The HITRAN 2008 molecular spectroscopic database, J. Quant. Spectrosc. Ra., 110, 533–572, 2009.

Scherer, M., Vömel, H., Fueglistaler, S., Oltmans, S. J., and Staehelin, J.: Trends and variability of midlatitude stratospheric water vapour deduced from the re-evaluated Boulder balloon series and HALOE, Atmos. Chem. Phys., 8, 1391–1402, doi:10.5194/acp-8-1391-2008, 2008.

Schwab, J. J., Pan, R.-J., and Zhang, J.: What constitutes a valid intercomparison of satellite and in situ stratospheric H_2O measurements?, J. Geophys. Res., 101, 1517–1528, doi:10.1029/95JD02999, 1996.

Solomon, S., Rosenlof, K. H., Portmann, R., Daniel, J., Davis, S., Sanford, T., and Plattner, G.-K.: Contribution of stratospheric water vapor changes to decadal variation in the rate of global warming, Science, 327, 1219–1222, 2010.

Stenke, A. and Grewe, V.: Simulation of stratospheric water vapor trends: impact on stratospheric ozone chemistry, Atmos. Chem. Phys., 5, 1257–1272, doi:10.5194/acp-5-1257-2005, 2005.

Taha, G., Thomason, L. W., and Burton, S. P.: Comparison of Stratospheric Aerosol and Gas Experiment (SAGE) II version 6.2 water vapor with balloon-borne and space-based instruments, J. Geophys. Res., 109, D18313, doi:10.1029/2004JD004859, 2004.

Thomason, L. W., Burton, S. P., Iyer, N., Zawodny, J. M., and Anderson, J.: A revised water vapor product for the Stratospheric Aerosol and Gas Experiment (SAGE) II version 6.2 data set, J. Geophys. Res., 109, D06312, doi:10.1029/2003JD004465, 2004.